# MATHEMATICAL MORPHOLOGY FOR DETECTING MARTIAN DUST DEVILS TRACKS AND INFERING THEIR MOVEMENT DIRECTIONS

*Morfologia Matemática para Detecção de Rastros de Dust Devils Marcianos e Inferência de suas Direções de Movimento*

**Thiago Statella**[1]
**Erivaldo Antônio da Silva**[2]

[1]**Instituto Federal de Educação, Ciência e Tecnologia de Mato Grosso – IFMT**
**Campus de Cuiabá - Depto. de área de Construção Civil**
Rua Zulmira Canavarros n° 95, Centro, Cuiabá-MT
thiago.statella@cba.ifmt.edu.br

[2]**Universidade Estadual Paulista – UNESP**
**Faculdade de Ciências e Tecnologia – FCT**
**Departamento de Cartografia**
Rua Roberto Simonsen n° 305, Presidente Prudente-SP
erivaldo@fct.unesp.br

## RESUMO

*Dust devils* são vórtices convectivos formados por correntes de ar quente instáveis, próximas às superfícies planetárias, provocadas por insolação. Eles têm sido estudados na Terra por séculos e foram observados pela primeira vez em Marte nas imagens orbitais do programa Viking. O conhecimento sobre sua atividade contribui para o entendimento do clima, geologia e evolução da superfície de Marte. Como exemplo, circulação de ar é um dos únicos processos ativos atualmente que modelam a superfície marciana e algumas pesquisas mostram que tais vórtices são responsáveis pela maioria das feições lineares e curvilineares do planeta. Além disso, a inferência da direção dos ventos baseada na detecção de rastros de *dust devils* por análise de imagens digitais é uma das poucas técnicas de verificação de modelos de circulação atmosférica marciana. Assim, este artigo enfoca a utilização de Morfologia Matemática para detectar, de maneira automática, rastros de *dust devils* e inferir suas direções principais. As áreas de estudo foram as regiões de *Argyre Planitia* e sudoeste de *Argyre*, capturadas em duas imagens obtidas pela câmera *Mars Orbiter Camera*, a bordo da sonda *Mars Global Surveyor*. As imagens foram pré-processadas para remoção de ruídos e em seguida foi aplicado um filtro top-hat para remover o gradiente de iluminação das cenas e realçar as feições de interesse. Os rastros de *dust devils* foram detectados por binarização automática e suas direções foram inferidas por análise granulométrica, com base no espectro padrão das feições detectadas.

**Palavras chaves:** Morfologia Matemática, Rastros de *dust devils*, Detecção de Feições.

## ABSTRACT

Dust devils are vortexes caused by unstable wind convection processes, near the surface, due to solar heat. They have been studied on Earth for centuries and were first observed on Mars in orbital images taken by the Viking program. Knowledge about their activity contributes to the understanding of Martian climate, geology and surface modification. As an example, the air circulation is one of the currently active process which models the surface of Mars and some researches show that these vortexes are responsible for most of the linear and curvilinear surface features of the planet. Moreover, the inference of the wind direction based on dust devils tracks detection, by digital image analysis, is one of the few techniques for verifying circulation models of the atmosphere. This paper is about using Mathematical Morphology to automatically detect dust devils tracks and infer their directions. The study areas were the regions of *Argyre Planitia* and Southwest of *Argyre*, depicted in two Mars Global Surveyor Mars Orbiter Camera images. The images were pre-processed in order to remove noise from radiometric distortions. Next, a top-hat filter was applied to remove illumination gradient from the scenes and to enhance the features of interest. Then, an automatic binarization algorithm was employed to detect dust devils tracks. Tracks directions were inferred by granulometric

analysis based on the spectrum of the morphological pattern of the detected features.

**Keywords:** Mathematical Morphology, Dust Devils Tracks, Feature Detection.

## 1. INTRODUCTION

Dust devils are vortexes caused by unstable wind convection processes near the planetary surfaces, due to solar heat. They have been studied on Earth for centuries and were first observed on Mars in orbital images taken by the Viking (1975), Mars Observer (1992) and Mars Pathfinder (1996) programs. These phenomena can achieve miles in width and height, and knowledge about their activity contributes to the understanding of Martian climate, geology and surface modification which is essential to plan future manned missions (BALME, WHELLEY and GREELEY, 2003; BALME and GREELEY, 2006). According to Örmo and Komatso (2003), air circulation is one of the currently active process which models the surface of Mars and some researches show that these vortexes are responsible for most of the linear and curvilinear surface features of the planet. Moreover, the inference of the wind direction based on dust devils tracks detection is one of the few techniques for verifying circulation models of the atmosphere. The Global Circulation Model (GCM) of the atmosphere indicates a wind behavior according to a pattern N-S and E-W, contrasting with directions inferred from dust devils tracks observation (SW-NE, NW-SE). This fact suggests that more research on aeolian processes is needed. The direction of dust devils tracks can be used to get information on wind circulation, and it can be done by image analysis (ÖRMO and KOMATSO, 2003; FENTON, TOIGO and RICHARDSON 2005).

In November 1996 NASA launched the mission Mars Global Surveyor (MGS) with the high resolution camera Mars Orbiter Camera (MOC) that took images of the planet between the years of 1997 to 2006 in a geometric resolution up to 1.5 m per pixel. There are hundreds of high resolution images depicting Martian surface, providing important data for, among others, researches in Geology, Cartography and Aeolian processes monitoring, at a level of detail never achieved before (BRIDGES *et al*., 2007; NASA, 1997). The amount of images taken (and therefore the amount of information on them) grew at a rate greater than the human capability to analyze and extract relevant information from these products to characterize the planet under study (BANDEIRA, SARAIVA and PINA, 2007). That made room for automatic feature extraction processes. This paper is about using Mathematical Morphology to automatically detect dust devils tracks and infer their directions, which contribute to a better understanding of wind circulation on mars surface. Images acquired by the Mars Orbiter Camera onboard Mars Global Surveyor depicting the regions of *Argyre Planitia* and Southwest of *Argyre* were used as study areas. Those images were pre-processed so that noise from radiometric distortions could be removed. Next, a top-hat filter was applied to remove illumination gradients from the scenes and to enhance the features of interest. Then, dust devils tracks could be detected by an automatic binarization. Track directions were inferred by granulometric analysis based on morphological pattern spectrum of the detected features.

## 2. MATHEMATICAL MORPHOLOGY

Mathematical Morphology (MM) is a tool for extracting image connected components which are useful for representing and describing the shape of a region, like edges, skeletons, convex hulls, etc., and it is also a tool for pre and post-processing, like filtering, thinning and pruning (GONZALEZ and WOODS, 2000). According to Goutsias and Heijmans (2000), the basic task when it comes to MM is to define non-linear operators to extract topologic or geometric information from images. It requires the development of a mathematical model for images and a rigorous theory to describe the properties of the operators. A digital image can be defined as follows:

**Definition1:** Let $E$ be a nonempty set of adjacent squares arranged in rows and columns, forming a rectangular surface. Let $K$ be a set of gray levels. A gray level image is a mapping $E \rightarrow K$. Usually, $K$ belongs to the interval [0, k] in $\mathbb{Z}$ with $E \in \mathbb{Z}^2$.

Mathematical Morphology is based on two major transformations, called *erosion* and *dilation*.

**Definition 2:** Let $B$ be a subset from $\mathbb{Z}^2$, $B \subset E$. The erosion of an image $f$ by $B$ is the minimum of the translation of $f$ by the vectors $-b$ of $B$. $B$ is called *Structuring Element* (SE).

$$\varepsilon_B(f) = \bigwedge_{b \in B} f_{-b} \qquad (1)$$

**Definition 3:** The dilation of $f$ by a SE $B$ is the maximum of the translation of $f$ by the vectors $-b$ of $B$.

$$\delta_B(f) = \bigvee_{b \in B} f_{-b} \qquad (2)$$

Details about the properties and application examples of erosion and dilation can be found in Serra (1986), Haralick et al. (1987), Facon (1996), Banon and Barrerra (1998) end Shih (2009).

The structuring element $B$ is a completely defined and known (size and shape) set which is

compared, in a transformation, to the image unknown set. The result of this transformation allows us to evaluate the unknown set (FACON 1996). Two basic shapes of SEs are given below (the bold position is the origin of the SE):

$$B_{cross} = \begin{bmatrix} 0 & 1 & 0 \\ 1 & \mathbf{1} & 1 \\ 0 & 1 & 0 \end{bmatrix},\ B_{box} = \begin{bmatrix} 1 & 1 & 1 \\ 1 & \mathbf{1} & 1 \\ 1 & 1 & 1 \end{bmatrix}. \qquad (3)$$

Based on erosion and dilation operators it is possible to define several morphological transformations as follows.

**Definition 4:** The opening $\gamma$ of $f$ by a structuring element $B$ is the erosion of $f$ by $B$ followed by a dilation by $B$ transposed (SOILLE, 2003):

$$\gamma_B(f) = \delta_{\check{B}}\left[\varepsilon_B(f)\right]. \qquad (4)$$

Openings properties can be found in Banon and Barrerra (1998). According to Soille (2003), a transformation having the same properties of the opening, but that cannot be written as a unique erosion followed by a dilation with the transposed SE, is called an algebraic opening. Matheron (1975) has shown that any algebraic opening can be defined as the supremum of a family of morphological openings. A powerful tool for filtering connected components is an algebraic opening called *surface area opening*.

**Definition 5:** The surface area opening $\gamma_\lambda$ is equivalent to the union of all openings with the connected SEs $B$ whose size in number of pixels equals $\lambda$ (Soille 2003):

$$\gamma_\lambda = \bigvee_i \left\{\gamma_{Bi} \mid B_i \text{ connected and } Area(B_i) = \lambda\right\}. \qquad (5)$$

**Definition 6:** The closing of $f$ by $B$ is the dilation of $f$ by $B$ followed by erosion using $B$ transposed (SOILLE, 2003):

$$\phi_B(f) = \varepsilon_{\check{B}}[\delta_B(f)]. \qquad (6)$$

Closings are *extensive* filters (a transformation $\Psi$ is extensive $\Leftrightarrow id \leq \Psi$, where $id$ is the identity transformation); so, it is possible to define a morphological operator based on subtraction that is named *top-hat by closing*.

**Definition 7:** The top-hat by closing operator is the difference between the closing of $f$ and $f$ itself:

$$\mu_B(f) = \phi_B(f) - f. \qquad (7)$$

The texture of components in binary images can be studied by a series of openings with a family of SEs convexes whose sizes increase at each iteration. This procedure is called *granulometry*.

**Definition 8:** Let $B \in \mathbb{Z}^2$ be a SE. The family $\Gamma = (\gamma_\lambda)_{\lambda \geq 0}$ of closings by scales $\lambda B = \{\lambda b \mid b \in B\}$, $\lambda \geq 0$, $B$ convex, is a granulometry.

The concept of a granulometry may be linked to the sieving of rocks in a gravel heap. The rocks are sieved through screens of increasing size, leaving only the rocks that are too big to pass through the sieve. This is analogous to the opening of an image using a particular size of SE. The residue after each opening is often collated into a granulometric curve. One currently used is the loss of surface area between $\gamma_\lambda$ and $\gamma_{\lambda+1}$ versus $\lambda$, which is known as *pattern spectrum*. In practice it is useful to assume $\lambda$ to be the radius of the SE (SOILLE, 2003). Besides size distribution, granulometry can be use to infer objects directions. To do that a family of line SEs $(L_\lambda)_{\lambda \geq 0}$ is considered. For a given pixel $p$, the directions to its neighbors (assuming 8 connectivity) $N_d(p)$, where $d$ = 0°, 45°,…,315°, are defined in Figure 1.

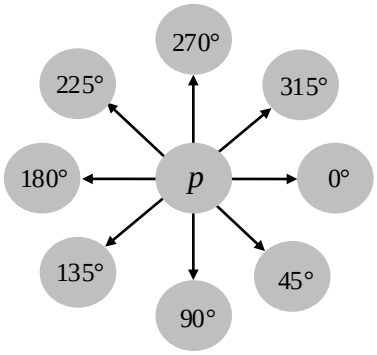


Fig. 1 - Directions of the 8 neighbors of $p$.

The direction opposed to $d$ is denoted $d'$, so if $d$ = 0° then $d'$ = 180°. The *path* in the direction $d$ is defined as the union of the radii of the SE in the directions $d$ and $d'$. As an example, the path in the direction 45° is composed by the radii (with origin in $p$) oriented to 45° and 225° (one can notice that the path in the direction 225° is identical to the path in the direction 45°, as both paths share the same radii). Now it is possible to define a family of line SEs whose paths are oriented in the directions 0°, 45°, 90° and 135°:

$$B_0 = \begin{bmatrix} 0 & 0 & 0 \\ 1 & \mathbf{1} & 1 \\ 0 & 0 & 0 \end{bmatrix},\ B_{45} = \begin{bmatrix} 1 & 0 & 0 \\ 0 & \mathbf{1} & 0 \\ 0 & 0 & 1 \end{bmatrix},$$
$$B_{90} = \begin{bmatrix} 0 & 1 & 0 \\ 0 & \mathbf{1} & 0 \\ 0 & 1 & 0 \end{bmatrix},\ B_{135} = \begin{bmatrix} 0 & 0 & 1 \\ 0 & \mathbf{1} & 0 \\ 1 & 0 & 0 \end{bmatrix}. \qquad (8)$$

More information on granulometry can be found in Schmitt (1991), Soille (2003) and Valero et al. (2010).

## 3. STUDY AREAS AND METHOD

Two portions of MOC images were chosen as study areas. They were obtained from the NASA database of the MGS mission. Figure 2 shows a portion of the image MOC2-220-A and Figure 3 shows a portion of the image E10-04279. Figure 4 shows the study areas on the surface of Mars. Table 1 summarizes informations about the study areas, like acquisition date, geodesic coordinates of images centers, geometric resolution, spectral band and martian geographical region to which they belong.

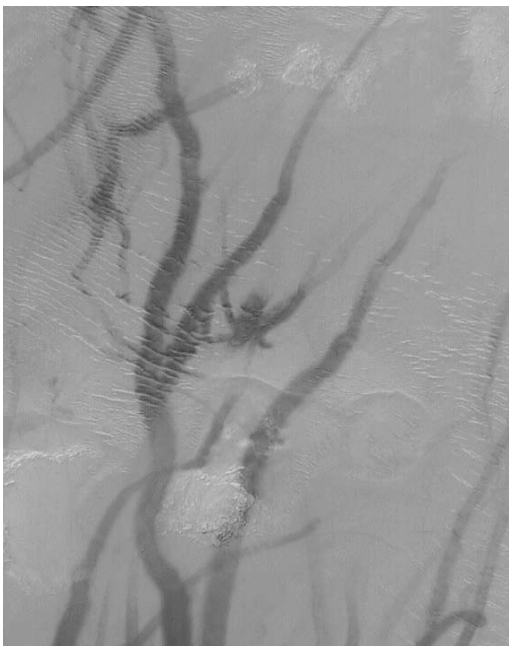

Fig. 2 – Image MOC2-220-A: Argyre Planitia.

The method developed to automatically detect dust devils tracks and to infer their directions is summarized in Figure 5. It is mainly based on two characteristics of the phenomena: 1) dust devils tracks are very dark features (a few references related white tracks but they are very rare, depending on the lithology), contrasting with the surrounding objects; 2) they are assumed to be the biggest objects in the images.

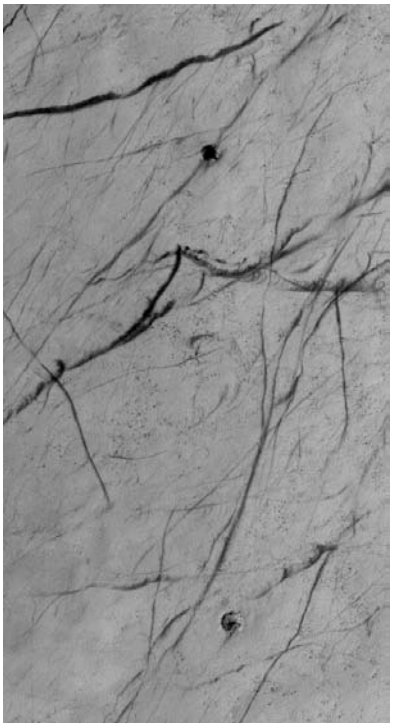

Fig. 3 – Image E10-04279: Southwest of Argyre.

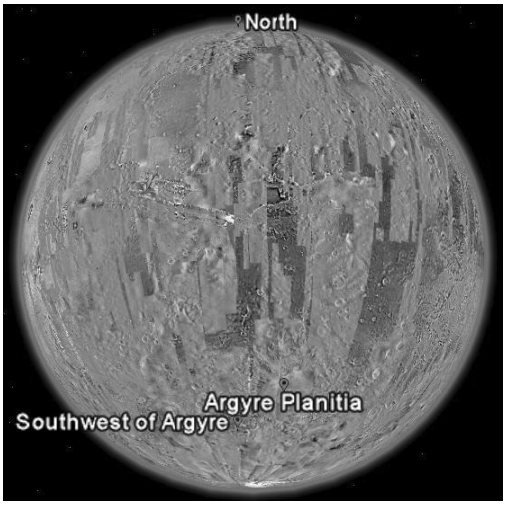


Fig. 4 – Study areas on Mars.

Besides, the tracks are topographically negative features, therefore appearing like valleys. So it is possible to enhance those features by applying a top-hat by closing filter.

Table 1 – Information about study areas.

| Name | Date | Lat° | Lon° | Res. | Size (pixels) | Band | Region |
|---|---|---|---|---|---|---|---|
| **MOC2-220-A** | 02/21/2000 | -51.3 | -41.3 | 6m | 566x714 | Pan* | Argyre Planitia |
| **E10-04279** | 11/27/2001 | -59.3 | -60.3 | 6m | 512x964 | Pan | Southwest Argyre |

*Pan stands for Panchromatic: $\lambda$ = 500 – 900 nm.

## 4. RESULTS AND DISCUSSION

According to Figure 5, the initial step is the suppression of noise and the attenuation of bright objects like sand dunes. In order to achieve that, the scenes were filtered by a median filter (3x3 mask) and by a surface area opening ($\lambda$ = 100 pixels). Next, the images were automatically binarized using the Otsu method (OTSU, 1979). A binarization is a transformation $T$ that maps gray levels from an image $f$ to the interval [0, 1] (where 0 (zero) is black and 1 (one) is white) in $T(f)$, based on a threshold $t$ which is generally chosen from histogram analysis. In the Otsu method, $t$ is chosen so that the interclass variance is maximized. The resulting images had the tracks in black and anything else in white. They were negated (the negative of a binary image is its complement: $neg(f) = 1-f$) so a granulometric analysis using openings could be done. At this step box-like SEs were used to infer the size of the biggest connected components in the study areas. As it can be seen from Figure 6, the radii of the SEs which removed the biggest connected components from images MOC2-220-A and E10-04279 were 27 pixels (Figure 6(*a*)) and 11 pixels (Figure 6(*b*)).

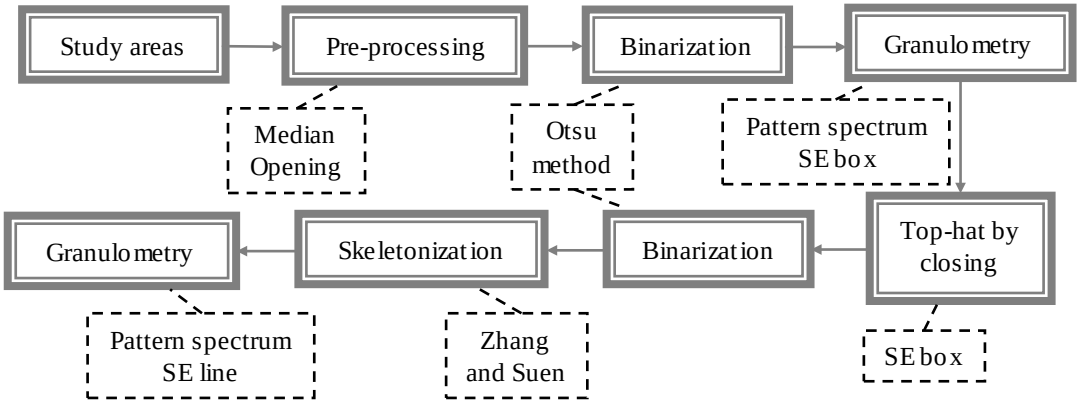


Fig. 5 - Flowchart of the method developed.

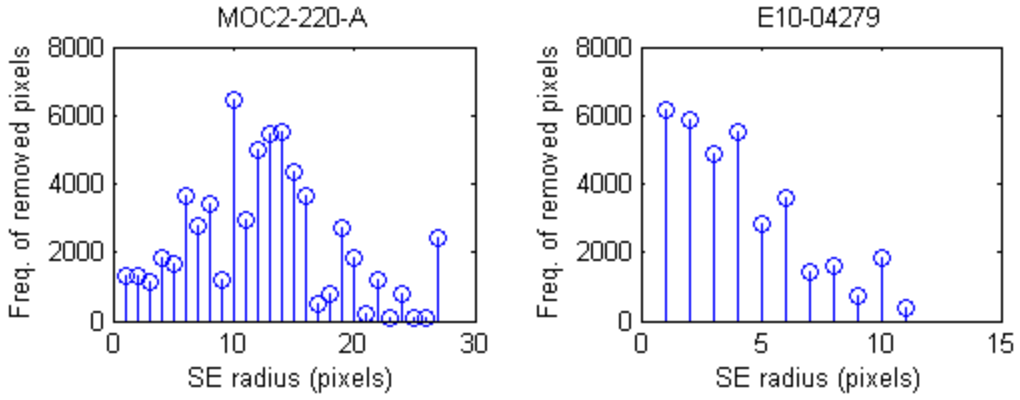


(*a*) (*b*)

Fig. 6 - Pattern spectrum with a SE box: (*a*) the biggest connected component was removed from scene with an opening by a SE whose radius was 27 pixels length; (*b*) in this case, when the radius of the SE was 11 pixels length the biggest connected component was removed.

Then top-hats by closing using SEs whose sizes were defined by the granulometry were applied to the filtered images to enhance the tracks (Figures 7 and 8, both shown with a linear contrast stretching) by removing scenes illumination gradients. A new binarization by the Otsu method was applied to detect the features (Figures 9 and 10) and a skeletonization was carried out. There are several ways of thinning a binary image (or even a gray level image). The method chosen here was the one proposed by Zhang and Suen (ZHANG and SUEN, 1984). This method avoids segmentation at the corner of objects (an undesired effect generally caused by other methods) and preserves the connectivity of the skeleton.

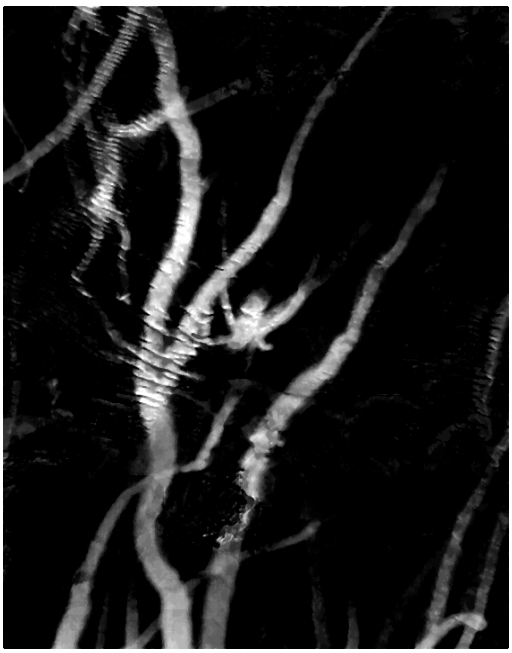

Fig. 7 – Image MOC2-220-A enhanced by top-hat.

A granulometric analysis was done over the skeletonization (this could have been done over the binary images but it would have caused errors due the thickness of the objects), this time using the family of SEs presented in (8). Figures 11 and 12 show the pattern spectrum of the scenes.

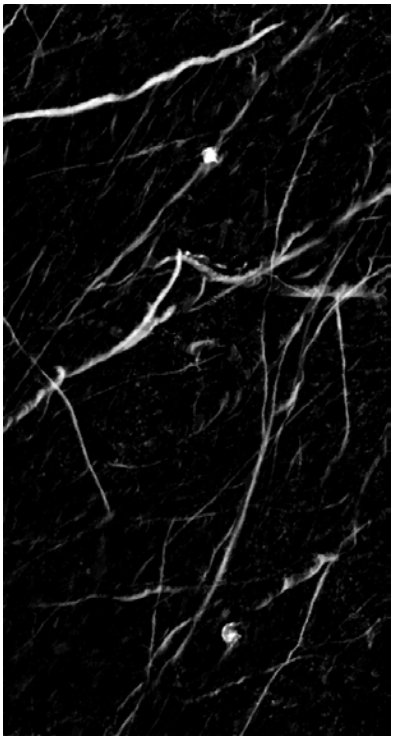

Fig. 8 – Image E10-04279 enhanced by top-hat.

For the MOC2-220-A image, as it can be seen from Figure 11, the frequency of pixels removed by openings with directional SEs was the highest (785 pixels removed) when the SE was oriented at 90°.

Figure 12 shows that, for E10-04279 image, the highest frequency of removed pixels (1,123 pixels removed) occurred when the SE was aligned with the path at 135°.

Fig. 9 – Dust devil tracks detected in MOC2-220-A.

Fig. 10 – Dust devil tracks detected in E10-04279.

Those are very good indicatives of the main direction followed by dust devils in the study areas. From binary images was also possible to determine the area covered by tracks for each scene. That resulted in

54,984 pixels for MOC2-220-A (~ 14% of the image) and 27,872 pixels for E10-04279 (~ 6% of the image).

## 5. CONCLUSION

Detecting dust devils tracks is a hard task for tracks that do not have specific orientation, length or thickness, so there is no easy way to predict and model their behavior. Besides, dust devils are very short time phenomena (they last a few minutes) and a lot of them can cross the same region in the same season, producing a number of overlapping streaks. Also, one can easily find fresh darker tracks (from recent phenomena) and weak smoothed tracks (from early phenomena) in a scene, which makes it difficult to detect the tracks. But if we think of those features as being the biggest and darker objects in the images then it is possible to enhance them by top-hat filtering. And we can find out their sizes and their main orientations by granulometric analysis. As it can be seen from Figures 9 and 10, tracks have been detected with a fairly good precision, except for the older and too much smoothed tracks. In such cases only a few streaks could be segmented. By making a visual analysis one can see that the main orientations were well identified. They resulted in N-S direction for MOC2-220-A image, which corresponds to the predicted direction of martian GCM; and SW-NE for E10-04279 image, which agrees with Örmo and Komatso (2003) and Fenton et al. (2005) observations. A final conclusion about dust devils main behavior cannot be done with only two study areas. Future work will apply the method in a greater number of images. This work was concerned in developing a method to detect dust devils tracks and infer their directions. The method is automatic and can be applied to images despite their resolution or the size of the tracks. The area covered by the tracks was also calculated from binary images. This is a good indicative of the frequency, intensity and size of dust devils crossing the study areas. The detected features and the information on their orientation can be compared to those predicted by GCM of Martian atmosphere and contribute to improve such models, as well as help to achieve a better understanding of mars climate. The results can also be used to map risk areas of the planet, improving Martian cartography.

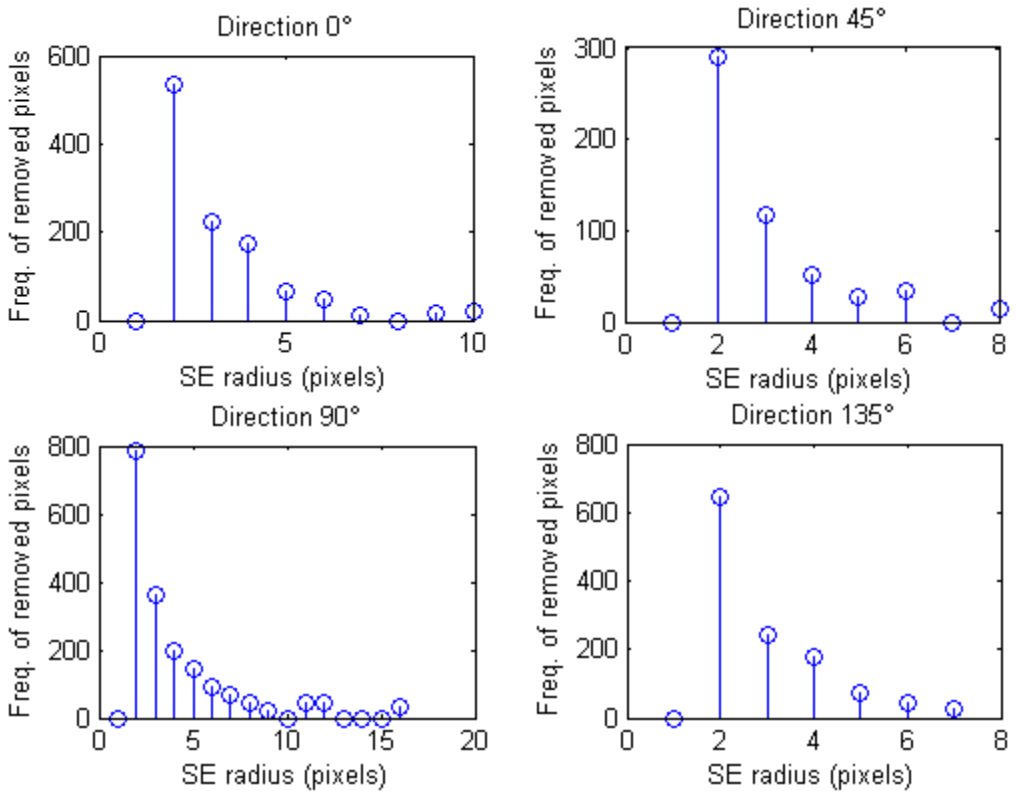


Fig. 11 - Pattern spectrum of MOC2-220-A. The highest frequency of removed pixels (785 pixels) was reached when the SE was aligned with the path at 90°.

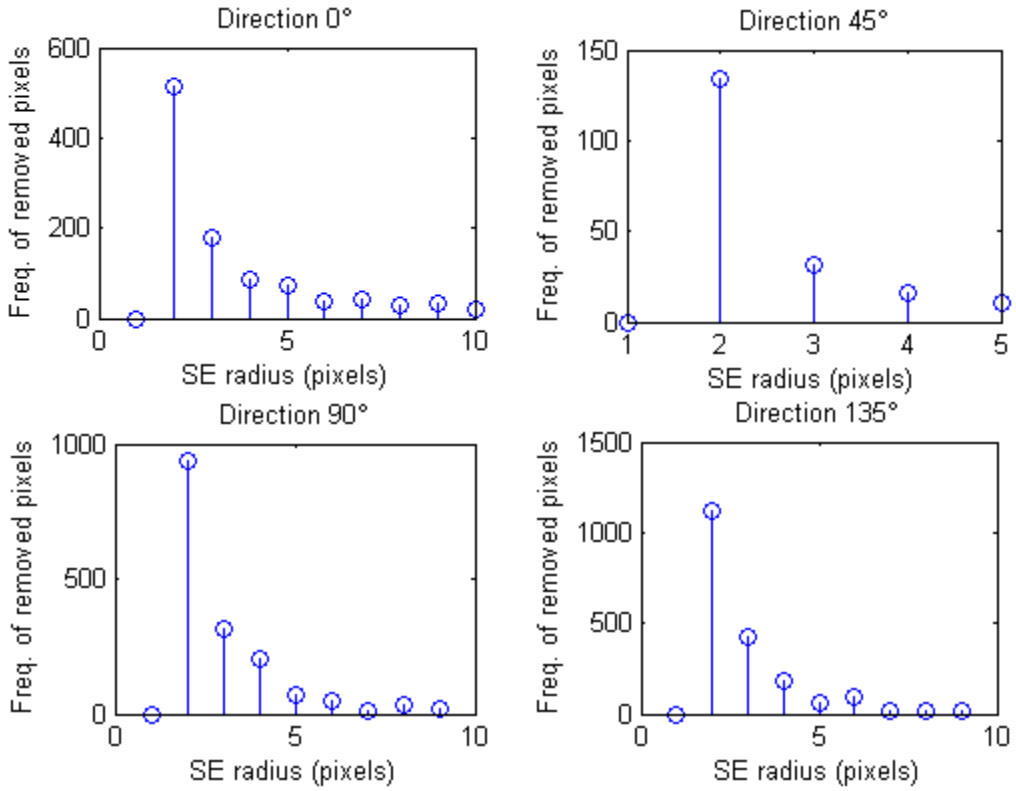


Fig. 12 - Pattern spectrum of E10-04279. The highest frequency of removed pixels (1,123 pixels) was reached when the SE was aligned with the path at 135°.

**REFERENCES**


BALME, M. R.; WHELLEY, P. L.; GREELEY, R. Mars: Dust devil track survey in Argyre Planitia and Hellas Basin. *Journal of Geophysical Research*, v. 108, n. E8, 2003.

BALME, M. R.; GREELEY, R. Dust Devils on Earth and Mars. *Reviews of Geophysics*, v. 44, 2006.

BANDEIRA, L.; SARAIVA, J.; PINA, P. Impact Crater Recognition on Mars Based on a Probability Volume Created by Template Matching. *IEEE Transactions on Geoscience and Remote Sensing*, v. 45, n. 12, p. 4008 – 4015, dez. 2007.

BANON, G. J. F.; BARRERA, J. *Bases da Morfologia Matemática para a análise de imagens binárias*, 2 ed. São José dos Campos: Instituto Nacional de Pesquisas Espaciais (INPE), 1998. 230p.

BRIDGES, N. T. et al. Aeolian Studies from HIRISE. In: XXXVIII Lunar and Planetary Science Conference 2007. *Anais do XXXVIII Lunar and Planetary Science Conference* 2007.

FACON, J. *Morfologia Matemática: teoria e exemplos*. Curitiba: PUC, 1996.

FENTON, L. K.; TOIGO, A. D.; RICHARDSON, M. I. Aeolian processes in Proctor Crater on Mars: Mesoscale modeling of dune-forming winds. *Journal of Geophysical Research*, v. 110, 2005.

GONZALEZ, R. C.; WOODS, R. E. *Processamento de Imagens Digitais*. São Paulo: Edgard Blucher LTDA, 2000. 508p.

GOUTSIAS, J.; HEIJMANS, H. J. A. M. Fundamenta Morphologicae Mathematicae. *Mathematical Morphology*: edição livro do periódico Fundamentae Informaticae, v. 41, n. 1-2, ISSN 0169-2968, Amsterdam: IOS Press, 2000. p. 1 – 31.

HARALICK, R. M.; STERNBERG S. R.; ZHUANG X. Image analysis using mathematical morphology. *IEEE Pattern Analysis and Machine Intelligence*, v. PAMI-9, n. 4, p. 532-555, Jul. 1987.

MATHERON, G. *Random sets and integral geometry*. Nova Iorque: Wiley, 1975. 261 p.

NASA. *Mars Global Surveyor Arrival*, Press kit. Nasa, 1997. Disponível em:<http://mars.jpl.nasa.gov/missions/past/globalsurveyor.html>. Acesso em: 17 jun. 2009.

ÖRMO, J.; KOMATSU, G. Mars Orbiter Camera observation of linear and curvlinear features in the Hellas basin: indications for multiple processes of formation. *Journal of Geophysical Research*, v. 108, 2003.

SCHMITT, M. Variations on a Theme in Binary Mathematical Morphology. *Journal of Visual Communication and Image Representation*, v. 2, n. 3, p. 244 – 258, 1991.

SERRA, J. Introduction to mathematical morphology. *Computer Vision, Graphics and Image Processing*, v. 35, n. 3, p. 283 – 305, 1986.

SHIH, F. Y. *Image processing and Mathematical Morphology: fundamentals and applications*. CRC, 2009. 439 p.

SOILLE, P. *Morphological Image Analysis*. 2 ed. Berlin: Springer-Verlag, 2003. 391 p.

VALERO, S. et al. Advanced Directional Mathematical Morphology for the Detection of the Road Network in Very High Resolution Remote Sensing Images. *Pattern Recognition Letters*, Elsevier, v. 31, n. 10, p. 1120 – 1127, 2010.